1 **Anticlockwise P-T evolution at ~280 Ma recorded from ultrahigh-temperature**

2 **metapelitic granulite in the Chinese Altai orogenic belt, a possible link with the Tarim**

3 **mantle plume?**

4

5 Laixi Tong[1], Yigang Xu[1], Peter A. Cawood [2], Xin Zhou[1, 3], Yibing Chen[1], Zhao Liu[1, 3]

6 1 State Key Laboratory of Isotope Geochemistry, Guangzhou Institute of Geochemistry,

7 Chinese Academy of Sciences, Guangzhou 510640, China

8 2 Department of Earth Sciences, University of St Andrews, Fife KY16 9AL, Scotland, UK

9 3 University of Chinese Academy of Sciences, Beijing 10049, China

10

11

12 **Abstract**

13 An ultrahigh-temperature (UHT) metapelitic granulite assemblage consisting of garnet(g)-

14 spinel(sp)-orthopyroxene(opx)-sillimanite(sil)-cordierite(cd)-ilmenite(ilm)-biotite(bi)-

15 plagioclase(pl)-quartz(q) occurs within migmatitic paragneiss near Kalasu in the Chinese

16 Altai, NW China. Textural relations, mineral compositions and P-T estimates, indicate three

17 stages of mineral assemblages: (1) pre-peak prograde stage (M1) consisting of a sp-sil-bearing

18 or sp-opx-bearing inclusion assemblage, with low-Al_2O_3 contents (4-5 wt %) in

19 orthopyroxene and P-T conditions of ~7 kbar and ~890 °C, (2) peak UHT stage (M2)

20 comprising a g-opx-cd-bearing coarse-grained assemblage, with high-Al_2O_3 contents (8-9

21 wt %) in orthopyroxene and peak conditions of ~8 kbar and ~970 °C, and (3) post-peak HT

22 stage (M3) containing an oriented opx-bi-sil-bearing assemblage in matrix, with moderate

23 amounts of Al_2O_3 (6-7 wt %) in orthopyroxene and P-T conditions of 8-9 kbar and ~870 °C.

24 The three discrete stages define an anticlockwise P-T path involving initial prograde heating

25 and post-peak near isobaric cooling. Such a near isobaric cooling anticlockwise P-T path

 *Corresponding author: State Key Lab of Isotope Geochemistry, Guangzhou Institute of Geochemistry, Chinese Academy
 of Sciences, Guangzhou 510640, China. Tel: +86 20 38383127, fax: +86 20 85290130.
 E-mail address: lxtong@gig.ac.cn (L. Tong)

26   suggests that UHT metamorphism might have occurred in an overall extensional tectonic

27   setting likely resulted from underplating of mantle-derived mafic magma. The SHRIMP

28   zircon U-Pb age of 278 ± 2 Ma obtained from the metapelitic granulite indicates UHT

29   metamorphism in the Altai orogen occurred during the Permian, coeval with spacially

30   associated mantle-derived mafic intrusions (~280 Ma) and the Tarim mantle plume (~275

31   Ma). Thus, the Permian UHT metamorphism of the Chinese Altai is likely associated with

32   underplating and heating of mantle-derived mafic magma as a result of the Tarim mantle

33   plume.

34

35   Key words: Ultrahigh-temperature metamorphism, the Chinese Altai, P-T path, U-Pb age,

36   mantle plume.

37

38

39   **1. Introduction**

40   The study of ultrahigh-temperature (UHT) metamorphism can provide important insight

41   into the formation and evolution process of deep continental crust (Harley, 2004). UHT

42   metamorphism involves very high temperature granulite-facies conditions in which crustal

43   rocks experienced peak temperature in excess of 900 °C, and is generally characterized by

44   mineral assemblages such as opx + sil + q, sa + q, crn + q, sp + q, and osm + g (sa, sapphirine;

45   crn, corundum; osm, osumilite), while the orthopyroxene contains over 8.0 wt% Al_2O_3

46   (Harley, 2004, 2008). The pressure range is mainly located in the sillimanite stability field

47   (Brown, 2007). Some 30 localities of UHT granulites have been reported worldwide; most are

48   restricted to Precambrian high-grade metamorphic terranes (Brown, 2007), including those in

49   East Antarctica, South India and North China (Raith et al., 1997; Harley and Motoyoshi, 2000;

50   Tong and Wilson, 2006; Santosh et al., 2007). As the UHT granulites contain important

51   information on the processes of lower crust evolution and possible crust-mantle interaction,

52 the study of these rocks is scientifically critical to understanding deep tectonothermal

53 evolution.

54   In the last several years, mafic and metapelitic granulites have been reported from the

55 Chinese Altai orogenic belt (Li et al., 2004; Chen et al., 2006a, 2006b; Wang et al., 2009).

56 Furthermore, Li et al. (2010) reported an occurrence of a UHT (>900 °C) metapelitic granulite

57 at Wuqiagou in Fuyun county. The P-T path of the UHT metapelitic granulite and the timing

58 of the UHT metamorphism are not yet resolved. Li et al. (2010) dated the UHT

59 metamorphism at ~499 Ma, whereas Li et al. (2012) gave its age as ~277 Ma. In this paper we

60 outline the petrography, P-T estimates and chronology of a garnet-orthopyroxene-sillimanite-

61 cordierite-bearing UHT granulite, documenting an anticlockwise P-T evolution path and

62 proposing that a synchronous mantle plume was responsible for the UHT metamorphism.

63

64 **2. Geological background**

65   The Altai orogenic belt constitutes part of the Central Asian Orogenic Belt, a

66 Neoproterozoic to late Palaeozoic accretionary orogen (Sengör et al., 1993; Jahn, 2004; Jahn

67 et al., 2004; Xiao et al., 2004, 2010; Cawood et al., 2009). The Altai orogenic belt is situated

68 on the south-western margin of the Siberian plate, and its southern boundary with the Junggar

69 plate is delineated by the large NW-trending Erqis fault (Fig. 1) (He et al., 1990; Windley et

70 al., 2002). The belt is divided into five fault-bounded terranes or tectonic units (He et al.,

71 1990; Windley et al., 2002; Xiao et al., 2004; Wang et al., 2006, 2009). Unit I and Unit II are

72 composed of the Devonian-Carboniferous volcanic-sedimentary rocks and Neoproterozoic-

73 Ordovician and minor Devonian sedimentary-volcanic rocks, respectively, and mostly

74 underwent greenschist facies metamorphism. Unit III (or the central Altai terrane) consists

75 largely of Neoproterozoic-Ordovician metasedimentary and metavolcanic rocks, with the

76 forms of a micro-continent block. The rocks in this unit generally experienced greenschist to

amphibolite facies metamorphism. Unit IV (or the Qiongkuer-Abagong terrane) contains late Silurian to early Devonian arc-type volcanic and pyroclastic rocks, displaying greenschist to upper amphibolite facies metamorphism and locally granulite facies conditions (Chen et al., 2006a; Wang et al., 2009; Li et al., 2010). Unit V (or the Erqis terrane) is composed of Precambrian basement and Devonian-Carboniferous volcaniclastic rocks, metamorphosed at greenschist to amphibolite facies conditions.

About 40 % of the Altai orogenic belt is composed of granitoids and orthogneiss consisting mainly of early Palaeozoic syn-orogenic and late Palaeozoic post-orogenic and anorogenic granitic bodies, which may be subdivided into tonalite, granodiorite and biotite granite, with minor two mica granite (Wang et al., 2006). The ages of the former are mainly around ~400 Ma (ranging from 450-370 Ma), and show a magmatic arc geochemical signature (Wang et al., 2006; Yuan et al., 2007; Sun et al., 2008), whereas the ages of the latter are mostly between 280 to 270 Ma (Wang et al., 2005; Tong et al., 2006a; Zhou et al., 2007; Zhang et al., 2010, 2012), and a mantle-derived geochemical signature (Tong et al., 2006b). Additionally, there are also some mantle-derived mafic intrusive rocks and ultramafic intrusive complex of about 280 Ma at Kalatongke and Wuqiagou in Fuyun county (Han et al., 2004; Chen and Han, 2006). These Permian ages are similar to the timing of movement on the Erqis shear zone (Laurent-Charvet et al., 2003; Briggs et al., 2007).

The Chinese Altai orogenic belt displays extensive development of Palaeozoic medium-low-pressure grade metamorphic zones and several granitic-gneissic thermal dome structures (Zhuang, 1994; Zhang et al., 2004; Xu et al., 2005; Wei et al., 2007). The metamorphic zones can be divided into kyanite-type and andalusite-type, and Windley et al. (2002) thought that the belt had features characteristic of a Barrovian-type metamorphic zone. The high-temperature portion in the andalusite-type zone develops a garnet-cordierite zone (Fig.1) (Zhuang, 1994; Wei et al., 2007), which reached granulite facies metamorphic conditions

(Wang et al., 2009). Zhuang (1994) reported an Rb-Sr whole-rock isochron of 365 Ma and Hu et al. (2002) a U-Pb zircon lower intercept age of 367 Ma from the gneisses in the region. These Devonian ages were interpreted to represent the time of the major greenschist-amphibolite facies metamorphism (Windley et al., 2002; Wei et al., 2007). More recently, zircon U-Pb age data further support early amphibolite facies metamorphism at 390-380 Ma (Long et al., 2007; Zheng et al., 2007; Jiang et al., 2010). This has led to two different opinions on the evolution history of the region: Devonian arc-continent collision (Windley et al., 2002; Wang et al., 2006; Wei et al., 2007), or a ridge-subduction and slab-window model accompanied by low-pressure high-temperature metamorphism (Windley et al., 2007; Sun et al., 2009; Jiang et al., 2010).

Additional zircon U-Pb and monazite Th-Pb ages of 290-260 Ma have been reported from the granulites or gneisses in the region (Hu et al., 2006; Chen et al., 2006b; Briggs et al., 2007; Zheng et al., 2007; Wang et al., 2009), indicating that the Altai orogenic belt experienced an important phase of high-grade structural metamorphic event in the late Palaeozoic (Xiao et al., 2006, 2008). For instance, Wang et al. (2009) recognized medium-low-pressure high-temperature (HT) (~800 °C) metapelitic granulites near Dakalasu of Aletai, and Li et al. (2010) reported a UHT (>900 °C) metapelitic granulite assemblage from Wuqiagou of Fuyun county, and conflicting ages of ~499 Ma and 270-290 Ma were obtained from the UHT metapelitic granulite (Li et al., 2010, 2012). Up to the present, different opinions still exist regarding the nature and its tectonic setting of the Permian high-grade metamorphic event, for instance, the Altai orogeny was subjected to an oceanic subduction and plate collision in the Permian that was responsible for the high-temperature or UHT granulite metamorphism (Chen et al., 2006a; Li et al., 2012), the Permian granulite facies metamorphism occurred in an extensional tectonic setting (Wang et al., 2009), or the Altai orogeny was associated with a Permian mantle plume event (Pirajno et al., 2008; Zhang et al., 2010; 2012).

127   The UHT metapelitic granulite sample (LT10F) presented in this study was collected near

128   Kalasu village, southeast of Aletai city (47°35′38′′N, 88°20′18′′E), occurring as rare tectonic

129   lenses within the medium-low-pressure garnet-cordierite-sillimanite-bearing metapelitic

130   granulite zone reported by Wang et al. (2009) (Fig. 2). Moreover, this metapelitic granulite

131   zone shows a feature of ductile shear deformation and contains small amounts of garnet-

132   bearing calcsilicate granulites, post-tectonic pegmatite veins, and Permian mafic intrusions

133   (Zhang et al., 2012). The UHT metapelitic granulites and medium-low-pressure metapelitic

134   granulites developed banded structures and generally experienced partial melting and

135   migmatitization, the latter of which display D1 folding and D2 shear fabrics.

136

137   **3. Petrography and mineral chemistry**

138   Minerals in the UHT metapelitic granulite (Table 1) were analyzed with a JXA-8100

139   microprobe at State Key Laboratory of Isotopic Geochemistry, Guangzhou Institute of

140   Geochemistry, Chinese Academy of Sciences, with an accelerating voltage of 15 kV, a beam

141   current of 3×10^{-8} Å, a beam width of 1 μm, and data correction by using a ZAF method.

142   Representative mineral compositions for the studied sample are listed in Table 1.

143   The UHT metapelitic granulite (LT10F) contains garnet (10%), orthopyroxene (7-8%),

144   cordierite (10-12%), sillimanite (2-3%), spinel (4-5%), biotite (15-20%), plagioclase (15-

145   20%), quartz (20-25%), and minor ilmenite and magnetite. No K-feldspar was observed in the

146   assemblages, which are similar to the mineral assemblages in the UHT metapelitic granulite at

147   Wuqiagou reported by Li et al. (2010). The petrographic observations show that the rock

148   develops at least two fabrics, S1 and S2 (Fig. 3a), probably in response to two episodes of

149   deformation D1 and D2. The S1 fabric consists mainly of coarse-grained less deformed

150   garnet-orthopyroxene-biotite-bearing mineral assemblage, whereas the S2 fabric is composed

151   of a mineral assemblage of biotite-orthopyroxene-sillimanite-plagioclase-quartz showing

152 marked preferred orientation (Figs. 3a & 3f). Coarse-grained cordierite grains contain spinel

153 and sillimanite inclusions (Fig. 3b), while garnet porphyroblast also contains spinel and

154 orthopyroxene inclusions (Fig. 3c). These textural relations suggest that the early M1

155 assemblage comprises spinel-sillimanite-bearing and spinel-orthopyroxene-bearing inclusion

156 assemblages. Peak M2 mineral assemblage is indicated by the coarse-grained less deformed

157 assemblage garnet-orthopyroxene-biotite-cordierite-plagioclase-quartz associated with

158 development of the S1 fabric (Figs. 3c & 3e). The orthopyroxene and spinel inclusions in the

159 garnet display retrograde biotite and cordierite, respectively (Fig. 3c), while some oriented

160 fine magnetite needles are also observed in the orthopyroxene grains (Fig. 3d). The M3

161 mineral association is indicated by the assemblage of orthopyroxene-biotite-sillimanite-

162 plagioclase±cordierite-magnetite-quartz showing marked preferred orientation in the matrix

163 (Fig. 3f).

164   Garnet compositions show an overall decrease in MgO content and a slight increase in CaO

165 content from core to rim (Fig. 4). In detail MgO content shows a slight increase (8.6 wt %)

166 and then decrease from the core (8.4 wt %) to the rim (6.7 wt %), with the corresponding X_{Mg}

167 (=Mg/(Fe^{2+}+Mg)) values of 0.346, 0.357 and 0.283, respectively. An orthopyroxene inclusion

168 has an X_{Mg} value of 0.609 and contains a low Al_2O_3 content (5.1 wt %) (as low as 4.5 wt %),

169 with a corresponding X_{Al} (=Al/2) value of 0.113 in the formula. Peak M2 orthopyroxene has

170 markedly higher Al_2O_3 contents than those of the M1 orthopyroxene inclusion and M3

171 orthopyroxene, and the core shows a highest Al_2O_3 content of 8.95 wt %, remarkably higher

172 than that of its rim (6.3 wt %), with the corresponding X_{Al} values of 0.199 and 0.141.

173 Cordierite is rich in MgO, with the X_{Mg} values of 0.855 and 0.837. Spinel inclusion has a

174 lower ZnO content (1.4 wt %) than that of matrix spinel (2.3 wt %), with the corresponding

175 X_{Mg} values of 0.437 and 0.294, respectively. Sillimanite contains an Fe_2O_3 content of 0.88

176 wt %. Biotite shows a decrease in TiO_2 content from the core (4.6 wt %) to the rim (3.8 wt %),

177   with resultant X_{Mg} values of 0.631 and 0.622, respectively. Anorthite contents in plagioclase

178   range from An_{31} to An_{46}.

179   In summary, that Al_2O_3 content exceeds 8.0 wt% in peak orthopyroxene indicates that peak

180   metamorphism in the metapelitic granulite reached UHT conditions (>900 °C) (Harley, 2004).

181   Moreover, the textural relations and mineral compositions show that three-stage mineral

182   assemblages can be distinguished: (1) pre-peak spinel-orthopyroxene-bearing or spinel-

183   sillimanite-bearing inclusion assemblage (M1), characterized by low Al_2O_3 contents (4-5

184   wt %) in orthopyroxene; (2) peak garnet-orthopyroxene-cordierite-K-feldspar-bearing UHT

185   mineral assemblage (M2), characterized by high Al_2O_3 contents (8-9 wt %) in orthopyroxene;

186   (3) post-peak orthopyroxene-sillimanite-biotite-magnetite-bearing HT mineral assemblage

187   (M3), with a feature of medium Al_2O_3 contents (6-7 wt %) in orthopyroxene.

188

189   **4. P-T Estimates and P-T path**

190   Equilibrated mineral pairs or mineral assemblages can be used to estimate the metamorphic

191   P-T conditions in the UHT metapelitic granulite, but many traditional garnet-orthopyroxene

192   thermobarometers fail to consider the effects of Fe^{2+}-Mg reset that can occur between mineral

193   pairs during the cooling after peak HT granulite facies metamorphism, and cannot give true

194   peak or pre-peak P-T conditions. Therefore, in this paper we adopt the garnet-orthopyroxene

195   thermobarometer corrected by Pattison et al. (2003) to estimate peak and pre-peak P-T

196   conditions of the studied UHT metapelitic granulite, and the average P-T method of Powell

197   and Holland (1994) is used to estimate the texturally equilibrated M3 mineral assemblage.

198   The P-T estimate results are listed in Table 2.

199   Low-Al orthopyroxene inclusion in garnet and the garnet in contact with the inclusion can

200   be used to estimate P-T conditions of pre-peak metamorphic stage (M1), and the calculated

201   results indicate that P-T conditions of pre-peak stage (M1) are ~7.0 kbar/~890 °C. Garnet

202 cores are inferred to have equilibrated with high-Al orthopyroxene, and thus their

203 compositions give estimates of the UHT formation conditions at the peak stage (M2), ~8.0

204 kbar/~970 °C. Because post-peak orthopyroxene-biotite-silllimanite-bearing HT mineral

205 assemblage (M3) does not contain garnet, and the garnet-orthopyroxene thermobarometer

206 cannot be used to estimate its P-T conditions. The average P-T calculation method of Powell

207 and Holland (1994) can be utilised to estimate post-peak HT formation conditions associated

208 with this assemblage (M3), and indicate P-T conditions of ~9.0 kbar/~870 °C (Table 2).

209 As the studied UHT metapelitic mineral assemblages contain magnetite and ilmenite, the

210 petrogenetic grid for the metapelites in the KFMASHTO model system (Fig. 5) (White et al.,

211 2002) can be used to better constrain the P-T evolution path of the UHT metapelitic granulite.

212 For instance, the above P-T conditions of three different metamorphic stages define an

213 anticlockwise P-T path of initial prograde heating and increase in pressure followed by a post-

214 peak near isobaric cooling (Fig. 5). P-T conditions of ~7.0 kbar/~890 °C for pre-peak spinel-

215 orthopyroxene-bearing or spinel-sillimanite-bearing inclusion assemblage (M1) are consistent

216 with the medium-low-pressure HT stability field that contains spinel-bearing assemblages in

217 the petrogenetic grid. Furthermore, P-T conditions of ~8.0 kbar/~970 °C for peak UHT

218 metamorphic stage (M2) are compatible with the high-Al feature (Al_2O_3 >8.0 wt%) in peak

219 orthopyroxene indicating a UHT metamorphic condition (>900 °C). P-T conditions of ~9.0

220 kbar/~870 °C for post-peak orthopyroxene-sillimanite-biotite-bearing HT mineral assemblage

221 (M3) are consistent with the medium-pressure HT stability field in the petrogenetic grid (Fig.

222 5). This suggests that if biotite and orthopyroxene-sillimanite-quartz are a paragenetic

223 association, they cannot be used to indicate a UHT metamorphic condition.

224 The above anticlockwise P-T path in the KFMASHTO system can very well explain the

225 development of mineral assemblages and textural relations in the UHT metapelitic granulite.

226 For example, several reactions that the P-T path crossed are mainly K-feldpar-consuming

227 reactions such as: (1) opx + cd + ksp + ilm + liq = g + bi + mt, and (2) g + cd + ksp + ilm =

228 opx + sil + bi + mt (Fig. 5). As reaction (2) progressed, K-feldspars broke down and

229 disappeared, and hence no K-feldspars preserved in the UHT metapelitic assemblages.

230 Oriented magnetite needles in peak Al-rich orthopyroxenes very likely formed through

231 exsolution during post-peak cooling, whereas the reaction (2) resulted in the formation of a

232 stable M3 mineral assemblage of orthopyroxene-sillimanite-biotite-magnetite-plagioclase-

233 quartz.

234

235 **5. P-T pseudosection calculation**

236   P-T pseudosection calculation for particular bulk compositions in a model system has been

237 widely used to infer metamorphic process and P-T path that produced mineral assemblages

238 and reaction textures in the metapelites, with the help of the Thermocalc program (Powell et

239 al., 1998; White et al., 2007). In this study, the mineral assemblages in the UHT metapelitic

240 granulite will be quantitatively modelled in the NCKFMASHTO system in order to constrain

241 its metamorphic P-T history. Following the method of White et al. (2007) for the metapelittes

242 with quartz and ilmenite in excess, a P-T pseudosection is then calculated for the mineral

243 assemblages in the UHT metapelitic granulite (LT10F) (Fig. 6).

244   The particular bulk composition for the UHT metapelitic granulite is estimated at first as

245 $H_2O : SiO_2 : Al_2O_3 : CaO : MgO : FeO : K_2O : Na_2O : TiO_2 : O = 0.30 : 55.82 : 13.13 : 1.58 :$

246 $11.91 : 13.54 : 1.40 : 1.23 : 0.72 : 0.68$, through bulk rock chemical analysis. The H_2O is set

247 such that the rock was just water saturated at the wet solidus (Tong and Wilson, 2006). The

248 calculated P-T pseudosection consists of various uni- and multi-variant equilibrated mineral

249 assemblages, and shows that peak M2 garnet-orthopyroxene-cordierite-K-feldspar-bearing

250 mineral assemblage formed under UHT conditions of 7-8 kbar and 900-980 °C, which are

251 further compatible with the peak M2 P-T conditions of ~8.0 kbar/~970 °C estimated from the

252   garnet-orthopyroxene thermobarometer (Fig. 6). Pre-peak spinel-orthopyroxene-bearing M1

253   inclusion assemblage is not well modelled, but orthopyroxene-bearing assemblage shows a

254   wide P-T range of 5-7 kbar and 850-950 °C, which are roughly consistent with the M1 P-T

255   estimates of ~7.0 kbar/~890 °C from thermobarometer. However, the P-T pseudosection

256   shows that post-peak orthopyroxene-biotite-sillimanite-magnetite-bearing M3 assemblage is

257   stable under conditions of 6-8 kbar and 700-870 °C, implying that the M3 P-T estimates from

258   thermobarometer may not be overestimated (Fig. 6). This is probably because that

259   orthopyroxene-biotite-sillimanite-magnetite-bearing M3 assemblage contains K-feldspar in

260   the NCKFMASHTO system makes the actual P-T stability field of the K-feldspar-absent M3

261   assemblage lower. Furthermore, the pseudosection also indicates that M3 assemblage might

262   contain late garnet. In summary, the P-T pseudosection calculated for the UHT metapelitic

263   granulite in this study apparently indicates a post-peak near-isobaric cooling anticlockwise P-

264   T path (Fig. 6). However, the absence of K-feldspar in the rock suggests that the P-T path

265   derived from the studied sample may be interpreted better by the P-T petrogenetic grid in the

266   KFMASHTO system (Fig. 5) than by the P-T pseudosection in the NCKFMASHTO system

267   (Fig. 6).

268

269   **6. SHRIMP zircon U-Pb ages**

270   Conventional magnetic and heavy liquid techniques followed by hand-picking under a

271   binocular microscope were used for separation of zircon. The morphology and internal

272   structure of the zircons were documented with transmitted and reflected light

273   microphotographs and cathodoluminescene (CL) images. The zircon grains were analysed

274   using the SHRIMP ion microprobe at the Beijing SHRIMP Centre, Chinese Academy of

275   Geological Sciences, using the standard operating conditions outlined by Williams (1998).

276   Th-U-Pb ratios were determined relative to the TEMORA standard zircon, and the absolute

277 abundances of U and Th relative to the SL13 standard zircon. Pb_c and Pb^* represent the

278 common and radiogenic portions, respectively, and common Pb was corrected using

279 measured ^{204}Pb. Software SQUID 1.0 and ISOPLOT (Ludwig, 1999) were used for data

280 processing. The weighted mean ages are quoted at the 95% confidence level.

281 Representative CL images of zircons in the UHT metapelitic granulite from the Altai

282 orogen are shown in Figure 7, and SHRIMP zircon U-Pb analysis data and age results are

283 listed in Table 3 and shown in Figure 8. Zircons in the UHT metapelitic granulite are euhedral

284 to semi-euhedral with length to width ratios of 2:1 to 4:1. Their images are mainly light gray

285 in colour, and lack magmatic oscillatory or rhythmic zoning (Fig. 7).

286 The Table 3 shows that the zircon ages are mostly distributed between 285-270 Ma, and

287 their calculated ^{206}Pb/^{238}U age is 278 ± 2 Ma (n = 33, MSWD = 1.2), with a weighted mean

288 age of 278 ± 2 Ma (Fig. 8). The Th/U ratios of the analysed zircons are relatively high,

289 ranging from 0.71 and 0.90. The CL imaging is consistent with the grains forming through

290 recrystallization during the UHT granulite metamorphism. Therefore, the U-Pb age of 278 ± 2

291 Ma should reflect the time of the UHT metamorphic event in the Chinese Altai orogenic belt.

292 This age shows a better precision than the U-Pb zircon age of 271 ± 5 Ma obtained recently

293 by the LA-ICP-MS technique from the same UHT metapelitic granulite in the study region

294 (Tong et al., 2013).

295

296 **7. Discussion**

297 Detailed petrographic observations, mineral compositions and P-T estimates, indicate the

298 existence of a garnet-orthopyroxene-sillimanite-cordierite-bearing UHT metapelitic granulite

299 near Kalasu, within the Altai orogenic belt. Peak orthopyroxene has an Al_2O_3 as high as 9.0

300 wt %, suggesting that peak metamorphism reached UHT conditions (>900 °C). P-T estimates

301 indicate peak metamorphic conditions of ~8.0 kbar/~970 °C, whereas P-T conditions of three

302   different metamorphic stages define an anticlockwise P-T path of initial prograde up-pressure

303   and heating and post-peak near isobaric cooling in the petrogenetic grid for the KFMASHTO

304   model system (White et al., 2002) (Fig. 5). The anticlockwise P-T path of post-peak near

305   isobaric cooling often reflects a tectonic process involving initial crustal compression

306   immediately followed by extension, and this process is normally accompanied by intrusions

307   of deep-derived magma or thinning of mantle lithosphere, which may provide an important

308   heat source resulting in rapid heating of thickening crust (Sandiford and Powell, 1991).

309   Therefore, the anticlockwise P-T path of post-peak near isobaric cooling obtained in this

310   study suggests that the Altai UHT metapelitic granulite might have formed in a tectonic

311   setting involving intrusions of deep-derived magma and accompanied by extensional heating

312   of the lower crust. This is consistent with the conclusion derived by Wang et al. (2009),

313   namely the medium-low-pressure HT metapelitic granulite formed in an extensional tectonic

314   setting of high heat flow.

315   The above results are contrasting with the inference from the UHT (>900 °C) metapelitic

316   granulite reported by Li et al. (2010) from Wuqiagou in Fuyun county (Fig. 1). They

317   considered that the UHT metapelitic granulite had a clockwise P-T path of post-peak

318   decompression that they considered to be associated with oceanic crustal subduction and plate

319   collision. Since the mineral assemblages and textural relations in the UHT metapelitic

320   granulites from the two areas are very similar, we think that the UHT metapelitic granulite at

321   Wuqiagou might have actually experienced an anticlockwise P-T history of post-peak near

322   isobaric cooling similar to that of this study. Furthermore, their so-called "clockwise P-T

323   path" has recently been changed to anticlockwise path (pers. comm. with Li Z., 2014). Li et al.

324   (2010) also undertook zircon dating for the UHT metapelitic granulite at Wuqiagou and

325   reported many grains gave ~500 Ma ages, which they suggested could be the age of either the

326   UHT metamorphic event or of an inherited source. Subsequently, Li et al. (2012) reported a

13

327 Permian zircon age (~277 Ma) in these rocks, which is identical within error to that in the

328 present study, supporting that the Altai UHT metamorphic event occurred in the Permian. The

329 timing of the UHT granulite facies metamorphic event is also compatible with the Permian

330 metamorphic ages (270-280 Ma) of other medium-low-pressure HT granulites and gneisses in

331 this orogenic belt (Table 4) (Chen et al., 2006b; Wang et al., 2009; Hu et al., 2006; Zheng et

332 al., 2007), suggesting a widespread Permian pulse of UHT and HT granulite facies

333 metamorphism in the Altai orogenic belt. As the UHT metapelitic granulite occurs as tectonic

334 lenses within the medium-low pressure high-temperature metapelitic granulites, this implies

335 that the UHT metapelitic granulite might have been emplaced into the medium-low pressure

336 high-temperature metapelitic granulites through D2 tectonism.

337 The Permian age of the Altai UHT metamorphic event is equivalent with the Permian

338 Tarim mantle plume activity in Xinjiang (~275 Ma) (Zhang et al., 2010), and is also well

339 compatible with the timing of the extensive Permian (280-260 Ma) mantle-derived mafic to

340 granitic magmatism that formed in a post-orogenic or anorogenic extensional setting in the

341 Altai region (Table 4) (Han et al., 2004; Chen and Han, 2006; Tong et al., 2006b; Briggs et al.,

342 2007; Zhang et al., 2012). Thus, the UHT metamorphism might have been caused by deeply

343 derived magma that heated the lower crust during extension and mantle plume activity in the

344 Permian. For instance, the post-orogenic or anorogenic Lamazhao granite and Fuyun granitic

345 dykes were respectively intruded at 276 ± 9 Ma and 275 ± 2 Ma (Wang et al., 2005; Tong et

346 al., 2006a), and they were derived from underplating of post-orogenic mantle-derived mafic

347 magma (Tong et al., 2006b), whilst the Kalatongke mafic intrusive complex (287 ± 5 Ma) in

348 Fuyun county was also considered to have formed during an underplating of mantle-derived

349 magma in a post-orogenic extensional setting (Han et al., 2004). Moreover, mantle-derived

350 Permian mafic intrusions also occur in the study area (Fig. 2). All these support the existence

351 of a Permian mantle plume activity (~275 Ma) in the Altai region (Pirajno et al., 2008; Zhang

352 et al., 2012). Therefore, the Altai UHT metamorphic event might be closely associated with

353 underplating of mantle-derived magma and extensional heating of lower crust caused by the

354 Permian Tarim mantle plume activity. In addition, the anticlockwise P-T paths recorded from

355 the granulites in the North China craton have been attributed to resulting from a mantle plume

356 activity (Zhao et al., 1999). Thus, this is not only consistent with the tectonic setting reflected

357 by the anticlockwise P-T path, but also compatible with the development of several granitic-

358 gneissic thermal dome structures in the Altai region (Zhuang, 1994).

359   Since the early amphibolite facies metamorphism in the Altai orogenic belt occurred in the

360 Devonian (Wei et al., 2007), this phase of metamorphism was ascribed to either an arc-

361 continent collision (Windley et al., 2002; Wang et al., 2006) or a ridge-subduction and slab-

362 window (Windley et al., 2007; Sun et al., 2009; Jiang et al., 2010), which formed the

363 framework of this orogenic belt. In this case, the Permian UHT metamorphic event is also

364 consistent with the time of the large Erqis shear zone (Briggs et al., 2007), along which the

365 voluminous A-type granites and anorogenic mafic intrusions emplaced at the same time

366 (Zhang et al., 2012). This suggests that the movement of the large Erqis shear zone was likely

367 coupling with the mantle plume activity, and was associated with an intraplate reworking.

368 Therefore, this Permian UHT metamorphism in the Chinese Altai orogen should reflect an

369 overprinting metamorphic event caused by the Permian Tarim mantle plume activity, rather

370 than a late Palaeozoic oceanic crustal subduction and plate collision that resulted in the HT or

371 UHT granulite metamorphism (Chen et al., 2006a; Li et al., 2012).

372

373 **8. Conclusions**

374   (1) Petrography, mineral compositions and metamorphic P-T estimates results for a garnet-

375 orthopyroxene-sillimanite-cordierite-bearing UHT metapelitic granulite from the Altai

376 orogenic belt near Kalasu, southeast of Aletai city, show an Al_2O_3 as high as 9.0 wt % in

377 orthopyroxene and peak P-T conditions of ~8.0 kbar and ~970 °C, and a post-peak near

378 isobaric cooling anticlockwise P-T path.

379   (2) The SHRIMP zircon U-Pb age dating yielded a concordant age of 278 ± 2 Ma, and

380 supported that the UHT metamorphic event in the Chinese Altai occurred in the Permian.

381   (3) The UHT metamorphic event occurred synchronously with the Permian (~280 Ma)

382 post-orogenic mantle-derived mafic intrusions related to the Permian (~275 Ma) Tarim mantle

383 plume activity, suggesting that the Permian UHT metamorphism in the Chinese Altai might

384 be closely associated with mantle underplating, heating and post-orogenic extension.

385

395

396 **References**

397 Briggs, S.M., Yin, A., Manning, C.E., Chen, Z.L., Wang, X.F., Grove, M., 2007. Late

398   Paleozoic tectonic evolution history of the Ertix Fault in the Chinese Altai and its

399   implications for the development of the Central Asian Orogenic System. GAS Bulletin

400   119, 944-960.

401 Brown, M., 2007. Metamorphic conditions in orogenic belts: a record of secular change.

402   International Geology Review 49, 193-234.

403   Cawood, P.A., Kröner, A., Collins, W.J., Kusky, T.M., Mooney, W.D. and Windley, B.F.,

404   2009. Accretionary Orogens through Earth history. In Cawood, P.A. and Kröner, A. (eds).

405   Earth Accretionary systems in Space and Time. Geological Society Special Publication

406   318, 1-36.

407   Chen, B., Jahn, B.-M., 2004. Genesis of post-collisional granitoids and basement nature of the

408   Junggar Terrane, NW China: Nd-Sr isotope and trace element evidence. Journal of Asian

409   Earth Sciences 23, 691-703.

410   Chen, H., Li, Z., Yang, S., Dong, C., Xiao, W., Tainosho, Y., 2006a. Mineralogical and

411   geochemical study of a newly discovered mafic granulite, northwest China: implications

412   for tectonic evolution of the Altay orogenic belt. Island Arc 15, 210-222.

413   Chen, H., Yang, S., Li, Z., Yu, X., Xiao, W., Yuan, C., Li, J., 2006b. Zircon SHRIMP U-Pb

414   chronology of the Fuyun basic granulite and its tectonic significance in the Altaid

415   orogenic belt. Acta Petrologica Sinica 22, 1351-58. (in Chinese with English abstract)

416   Chen, L., Han, B., 2006. Geochronology, geochemistry and Sr-Nd-Pb isotopic composition of

417   mafic intrusive rocks in Wuqiagou area, north Xinjiang: constraints for mantle sources

418   and deep processes. Acta Petrologica Sinica 22, 1201-1214. (in Chinese with English

419   abstract)

420   Han, B., Ji, J., Song, B., Chen, L., Li, Z., 2004. SHIMP zircon U-Pb age of Kalatongke No.1

421   and Huangshandong Cu-Ni-bearing mafic-ultramafic complexes, North Xinjiang, and

422   geological implications. Chinese Science Bulletin 49, 2424-2429.

423   Harley, S.L., 2004. Extending our understanding of ultrahigh temperature crustal

424   metamorphism. Journal of Mineralogical and Petrological Science 99, 140-158.

425   Harley, S.L., 2008. Refining the P-T records of UHT crustal metamorphism. Journal of

426   Metamorphic Geology 26, 125-154.

427   Harley, S.L., Motoyoshi, Y., 2000. Al zoning in orthopyroxene in a sapphirine quartzite:

428   evidence for >1120 °C UHT metamorphism in the Napier Complex, Antarctica, and

429   implications for the entropy of sapphirine. Contributions to Mineralogy and Petrology 138,

430   293-307.

431   He, G., Han, B., Yue, Y., Wang, J., 1990. Tectonic division and crustal evolution of Altay

432   orogenic belt in China. Geoscience of Xinjiang 2, 9-20. (in Chinese with English abstract)

433   Hu, A., Zhang, G., Zhang, Q., Li, T., Zhang, J., 2002. A review on ages of Precambrian

434   metamorphic rocks from Altai orogen in Xinjiang, NW China. Chinese Journal of

435   Geology 37, 129-142. (in Chinese with English abstract)

436   Hu, A., Wei, G., Deng, W., Chen, L., 2006. SHRIMP zircon U-Pb dating and its significance

437   for gneisses from the southwest area to Qinghe county in Xinjiang, NW China. Acta

438   Petrlogica Sinica 22, 1-20. (in Chinese with English abstract)

439   Jahn, B.-M., 2004. The Central Asian Orogenic Belt and growth of the continental crust in the

440   Phanerozoic. In: Malpas, J., Fletcher, C.J.N., Ali, J.R., Aitchison, J.C., (eds), Aspects of

441   the Tectonic Evolution of China, Geological Society Special Publications 226, 73-100.

442   Jahn, B.-M., Windley, B., Natal'in, B, Dobretsov, N., 2004. Phanerozoic continental growth

443   in Central Asian. Journal of Asian Earth Sciences 23, 599-603.

444   Jiang, Y., Sun, M., Zhao, G., Yuan, C., Xiao, W., Xia, X., Long, X., Wu, F., 2010. The ~390

445   Ma high-*T* metamorphic event in the Chinese Altai: a consequence of ridge-subduction?

446   American Journal of Science 310, 1421-1452.

447   Laurent-Charvet, S., Charvet, J., Monie, P., Shu, L., 2003. Late Paleozoic strike-slip shear

448   zones in eastern central Asia (NW China): new structural and geochronological data.

449   Tectonics 22, 1009, doi:10.1029/2001TC901047

450   Li, Z., Chen, H., Yang, S., Xiao, W., Tainosho, Y., 2004. Discovery of the basic granulite

451   from the Altai area: evidence from mineralogy. Acta Petrologica Sinica 20, 1445-55. (in

452   Chinese with English abstract)

453   Li, Z., Li, Y., Chen, H., Santosh, M., Xiao, W., Wang, H., 2010. SHRIMP U-Pb zircon

454   chronology of ultrahigh-temperature spinel-orthopyroxene-garnet granulite from south

455   Altay orogenic belt, Northwestern China. Island Arc 19, 506-516.

456   Li, Z., Li Y., Wang, H., Chen, H., Yang, X., 2012. Late Palaeozoic ultrahigh temperature

457   metamorphism of the Altai and its evolution. 2012 National Symposium on Petrology and

458   Geodynamics (abst), p. 319. (in Chinese)

459   Long, X., Sun, M., Yuan, C., Xiao, W., Lin, S., Wu, F., Xia, X., Cai, K., 2007. Detrital zircon

460   age and Hf isotopic studies for metasdimentary rocks from the Chinese Altai: implications

461   for the early Paleozoic tectonic evolution of the central Asian orogenic Belt. Tectonics 26,

462   TC5015, doi: 10.1029 /2007TC002128

463   Ludwig, K.R., 1999. Using Isoplot/EX, version 2. A Geological Toolkit for Microsoft Excel.

464   Berkeley Geochronological Center, Special Publication 1a, p. 47.

465   Pattison, D.M., Chacko, T., Farquhar, J., McFarlane, C.R.M., 2003. Temperatures of

466   granulite-facies metamorphism: constraints from experimental phase equilibria and

467   thermobarometry corrected for retrograde exchange. Journal of Petrology 44, 867-900.

468   Pirajno, F., Mao, J., Zhang, Z., Zhang, Z., Chai, F., 2008. The association of mafic- ultramafic

469   intrusions and A-type magmatism in the Tian Shan and Altay orogens, NW China:

470   implications for geodynamic evolution and potential for the discovery of new ore deposits.

471   Journal of Asian Earth Sciences 32, 165-183.

472   Powell, R., Holland, T., 1994. Optimal geothermometr and geobarometry. American

473   Mineralogist 79, 120-133.

474   Powell, R., Holland, T., Worley, B., 1998. Calculating phase diagrams involving solid

475   solutions via non-linear equations, with examples using THERMOCALC. Journal of

476   Metamorphic Geology 16, 577-588.

477   Raith M, Karmakar S and Brown M. 1997. Ultrahigh-temperature metamorphism and multi-

478   stage decompressional evolution of sapphirine-granulites from Palni hill ranges, southern

479   India. Journal of Metamorphic Geology 15, 379-399.

480   Sandiford, M., Powell, R., 1991. Some remarks on high-temperature-low-pressure

481   metamorphism in convergent orogens. Journal of Metamorphic Geology 9, 333-340.

482   Santosh, M., Tsunogae, T., Li, J., Liu, S., 2007. Discovery of sapphirine-bearing Mg-Al

483   granulites in the north China Craton: implications for Palaeoproterozoic ultrahigh-

484   temperature metamorphism. Gondwana Research 11, 263-285.

485   Sengör, A.M.C., Natal'in, B.A., Burtman, V.S., 1993. Evolution of the Altaid tectonic collage

486   and Palaeozoic crustal growth in Eurasia. Nature 54, 117-137.

487   Sun, M., Yuan C, Xiao W, Long X, Xia X, Zhao G, Lin S, Wu F, Kroner, A., 2008. Zircon U-

488   Pb and Hf isotopic study of gneissic rocks from the Chinese Altai: progressive

489   accretionary history in the early to middle Paleozoic. Chemical Geology 247, 352-383.

490   Sun, M., Long, X., Cai, K., Jiang, Y., Wang, B., Yuan, C., Zhao, G., Xiao, W., Wu, F., 2009.

491   Early Palaeozoic ridge subduction in the Chinese Altai: insight from the abrupt change in

492   zircon Hf isotopic compositions. Science in China (series D) 52, 1345-1348.

493   Tong, L., Wilson, C.J.L., 2006. Tectonothermal evolution of the ultrahigh temperature

494   metapelites in the Rauer Group, east Antarctica. Precambrian Research 149, 1-20.

495   Tong, Y., Hong, D., Wang, T., Wang, S., Han, B., 2006a. TIMS U-Pb zircon ages of Fuyun

496   post-orogenic linear granite plutons on the southern margin of Altay orogenic belt and

497   their implications. Acta Petrologica et Mineralogica 25, 85-89. (in Chinese with English

498   abstract)

499   Tong, Y., Wang, T., Hong, D., Han, B., 2006b. Pb isotopic compositions of granitoids from

500   the Altay Orogen (China): evidence for mantle-derived origin and continental growth.

501   Acta Geologica Sinica 40, 517-528. (in Chinese with English abstract)

502   Tong, L., Chen, Y., Xu, Y., Zhou, X., Liu, Z., 2013. Zircon U-Pb ages of the ultrahigh-

503   temperature metapelitic granulite from the Altai orogeny, NW China, and geological

504   implications. Acta Petrologica Sinica 29, 3435-3445. (in Chinese with English abstract)

505   Wang, T., Hong, D., Tong, Y., Han, B., Shi, Y., 2005. Zircon U-Pb SHRIMP age and origin

506   of post-orogenic Lamazhao granite pluton from Altai orogen: its implications for vertical

507   continental growth. Acta Petrologica Sinica 21, 640-650. (in Chinese with English

508   abstract)

509   Wang, T., Hong, D., Jahn, B.-M., Tong, Y., Wang, Y., Han, B., Wang, X., 2006. Timing，

510   petrogenesis, and setting of Paleozoic synorogenic intrusions from the Altai Mountains,

511   Northwest China: implications for the tectonic evolution of an accretionary orogen.

512   Journal of Geology 114, 735-751.

513   Wang, T., Jahn, B.-M., Kovach, V.P., Tong, Y., Hong, D., Han, B., 2009. Nd-Sr isotopic

514   mapping of the Chinese Altai and implications for continental growth in the central Asian

515   orogenic Belt. Lithos 110, 359-372.

516   Wang, W., Wei, C., Wang, T., Lu, Y., Chu, H., 2009. Determination of pelitic granulites in

517   the Chinese Altai orgenic belt and geological implications. Chinese Science Bulletin 54,

518   918-923. (in Chinese)

519   Wei, C., Clarke, G., Tian, W., Qiu, L., 2007. Transition of metamorphic series from the

520   kyanite- to andalusite-types in the Altai orogen, Xinjiang, China: evidence from

521   petrography and calculated KMnFMASH and KFMASH phase relations. Lithos 96, 353-

522   374.

523   White, R.W., Powell, R., Clarke, G.L., 2002. The interpretation of reaction textures in Fe-rich

524   metapelitic granulites of the Musgrave Block, central Australia: constraints from mineral

525   equilibria calculations in the system K_2O-FeO-MgO-Al_2O_3-SiO_2-H_2O-TiO_2-Fe_2O_3.

526   Journal of Metamorphic Geology 20, 41-55.

527 White, R.W., Powell, R., Holland, T.J.B., 2007. Progress related to calculation of partial

528 melting equilibria for metapelites. Journal of Metamorphic Geology 25, 511-527.

529 Williams, I.S., 1998. U-Th-Pb geochronology by ion microprobe. Reviews on Economic

530 Geology 7, 1-35.

531 Windley, B.F., Kroner, A., Guo, J., Qu, G., Li, J., Zhang, C., 2002. Neoproterozoic to

532 Paleozoic geology of the Altai orogen, NW China: new zircon age data and tectonic

533 evolution. Journal of Geology 110, 719-737.

534 Windley, B.F., Alexeiev, D., Xiao, W., Kroner, A., Badarch, G., 2007. Tectonic models for

535 accretion of the Central Asian Orogenic belt. Journal of the Geological Society, London

536 164, 31-47.

537 Xiao, W., Windley, B.F., Badarch, G., Sun, S., Li, J., Qin, K., Wang, Z., 2004. Palaeozoic

538 accretion and convergent tectonics of the southern Altaids: implications for the growth of

539 Central Asia. Journal of the Geological Society, London 161, 339-342.

540 Xiao, W., Han, C., Yuan, C., Chen, H., Sun, M., Lin, S., Li, Z., Mao, Q., Zhang, J., Sun, S., Li,

541 J., 2006. Unique Carboniferous-Permian tectonic-metallogenic framework of northern

542 Xinjiang (NW China): constraints for the tectonics of the southern Palaoasian domain.

543 Acta Petrologica Sinica 22, 1062-76. (in Chinese with English abstract)

544 Xiao, W., Han, C., Yuan, C., Sun, M., Lin, S., Chen, H., Li, Z., Li, J., Sun, S., 2008. Middle

545 Cambrian to Permian subduction-related accretionary orogenesis of Northern Xinjiang,

546 NW China: implications for the tectonic evolution of central Asia. Journal of Asian Earth

547 Sciences 32, 102-117.

548 Xiao, W., Huang, B., Han, C., Sun, S., Li, J., 2010. A review of the western part of the

549 Altaids: a key to understanding the architecture of accretionary orogens. Gondwana

550 Research 18, 253-273.

551 Xu, X., Zheng, C., Zhao, Q., 2005. Metamorphic types and crustal evolution of Hercynian

552   orogenic belt in Altai region, Xinjiang. Journal of Jilin University 35, 7-11. (in Chinese

553   with English abstract)

554 Yuan, C., Sun, M., Xiao, W., Li, X., Chen, H., Lin, S., Xia, X., Long, X., 2007. Accretionary

555   orogenesis of the Chinese Altai: insights from Palaeozoic granitoids. Chemical Geology

556   242, 22-39.

557 Zhang, C., Wei, C., Qiu, L., 2004. Evolution of metamorphism and its geologic significance

558   in Altaids, Xinjiang. Xinjiang Geology 22, 16-23. (in Chinese with English abstract)

559 Zhang, C.L., Li, Z.X., Li, X.H., Xu, Y.G., Zhou, G., Ye, H.M., 2010. A Permian large

560   igneous province in Tarim and Central Aisian orogenic belt, NW China: results of a ca.

561   275 Ma mantle plume? Geologic Society of America Bulletin 122, 2020-2040.

562 Zhang, C.L., Santosh, M., Zou, H.B., Xu, Y.G., Zhou, G., Dong, Y.G., Ding, R.F., Wang,

563   H.Y., 2012. Revisiting the "Irtish tectonic belt": implications for the Palaeozoic tectonic

564   evolution of the Altai orogen. Journal of Asian Earth Sciences 52, 117-133.

565 Zhao, G., Wilde, S.A., Cawood, P.A., Lu, L., 1999. Thermal evolution of two textural types

566   of mafic granulites in the North China craton: evidence for both mantle plume and

567   collisional tectonics. Geological Magazine 136, 223-240.

568 Zheng, C.Q., Kato, T., Enami, M., Xu, X.C., 2007. CHIME monazite ages of metasediments

569   from the Altai orogen in northwestern China: Devonian and Permian ages of

570   metamorphism and their significance. Island Arc 16, 598-604.

571 Zhou, G., Zhang, Z.C., Luo, S.B., He, B., Wang, X., Ying, L.J., Zhao, H., Li, A.H., He, Y.K.,

572   2007. Confirmation of high-temperature strongly peraluminous Mayin'ebo granites in

573   the margin of Altay, Xinjiang: age, geochemistry and tectonic implications. Acta

574   Petrologica Sinica 23, 1909-1920. (in Chinese with English abstract)

575 Zhou, M.F., Lesher, C.M., Yang, Z., Li, J., Sun, M., 2004. Geochemistryand petrogenesis of

576   270 Ma Ni-Cu-(PGE)sulfide-bearing mafic intrusions in the Huangshan district, eastern

577 Xinjiang, northwest China: implications for the tectonic evolution of the central Asian

578 orogenic belt. Chemical Geology 209, 233-257.

579 Zhuang, Y., 1994. The PTSt evolution of metamorphism and development mechanism of the

580 thermal structural gneiss domes in the Chinese Altaides. Acta Geologica Sinica 68. 35-47.

581 (in Chinese with English abstract)

582

583 **Figure Captions**

584 **Fig. 1** Metamorphic map of the Chinese Altai orogen (modified after Wei et al., 2007).

585

586 **Fig. 2** Metamorphic map of the study area, showing the sample location, and symbols are

587 same as those of the Figure 1.

588

589 **Fig. 3** Textural relations of the UHT metapelitic granulite in the Chinese Altai, in which (a),

590 (b), (c), (e) and (f) are microphotographs in plane-polarized light, but (d) is backscattered

591 image. (a) two phases of gneissic foliation S1 and S2 defined by different orientation of

592 biotite flakes, and garnet contains biotite and ilmenite inclusions; (b) cordierite contains

593 spinel and sillimanite inclusions; (c) garnet porphyroblast contains orthopyroxene and

594 spinel inclusions, with retrograde biotite and cordierite around them, respectively; (d)

595 Al-rich orthopyroxene contains oriented acicular magnetite; (e) equilibrated peak

596 assemblage g-bi-opx-pl-cd-q; (f) M2 mineral assemblage opx-bi-sil-mt-pl-q showing

597 marked preferred orientation. Mineral abbreviations: g, garnet; opx, orthopyroxene; sil,

598 sillimanite; cd, cordierite; sp, spinel; bi, biotite; pl, plagioclase; ilm, ilmenite; mt,

599 magnetite; q, quartz.

600

601 **Fig. 4** Composition variation diagram of a garnet porphyroblast from core to rim.

602

603 **Fig. 5** P-T projection in the KFMASHTO system for metapelites, showing the P-T path of the

604 UHT metapelitic granulite in the Chinese Altai orogen (after White et al., 2002). Mineral

605 abbreviations: ksp, K-feldspar; ky, kyanite; mu, muscovite; ru, rutile; liq, melt; others are

606 same as those in Fig. 2.

607

608 **Fig. 6** P-T pseudosection calculated for the studied UHT metapelitic granulite in the model

609 NCKFMASHTO system with quartz and ilmenite in excess.

610

611 **Fig. 7** The CL images for representative zircons in the UHT metapelitic granulite.

612

613 **Fig. 8** U-Pb concordant age diagram for zircons in the UHT metapelitic granulite.

614

615 **Table Captions**

616 **Table 1** The EPMA analysis results of representative minerals in the UHT metapelitic

617 granulite (wt%), in which Fe_2O_3 and FeO contents are recalculated assuming

618 stoichiometry.

619 Abbreviations: g(c), garnet core; g(m), middle garnet between core and rim; g(r),

620 garnet rim; opx(i), orthopyroxene inclusion in garnet; opx(c), orthopyroxene core;

621 opx(m), middle orthopyroxene between core and rim; opx(r), orthopyroxene rim;

622 opx(2), M2 orthopyroxene; ilm(i), ilmenite inclusion; sp(i), spinel inclusion; sp(o),

623 spinel in matrix; mt(e), magnetite needle in orthopyroxene; cd(i), cordierite inclusion;

624 bi(i), biotite inclusion; bi(c), biotite core; bi(r), biotite rim. $X_{Mg}=Mg/(Fe^{2+}+Mg)$;

625 $X_{Al}=Al/2$.

626

627   **Table 2** P-T estimate results for three-stage mineral assemblages in the UHT metapelitic

628   granulite. The corrected garnet-orthopyroxene thermobarometers of Pattison et al.

629   (2003) are applied for estimating M1 and M2 P-T conditions, while the average P-T

630   method of Powell and Holland (1994) is used for M3 P-T estimates. The fit value for

631   M3 P-T estimates is less than 1.61, suggesting that the average P-T calculation falls

632   within 95% confidence level.

633

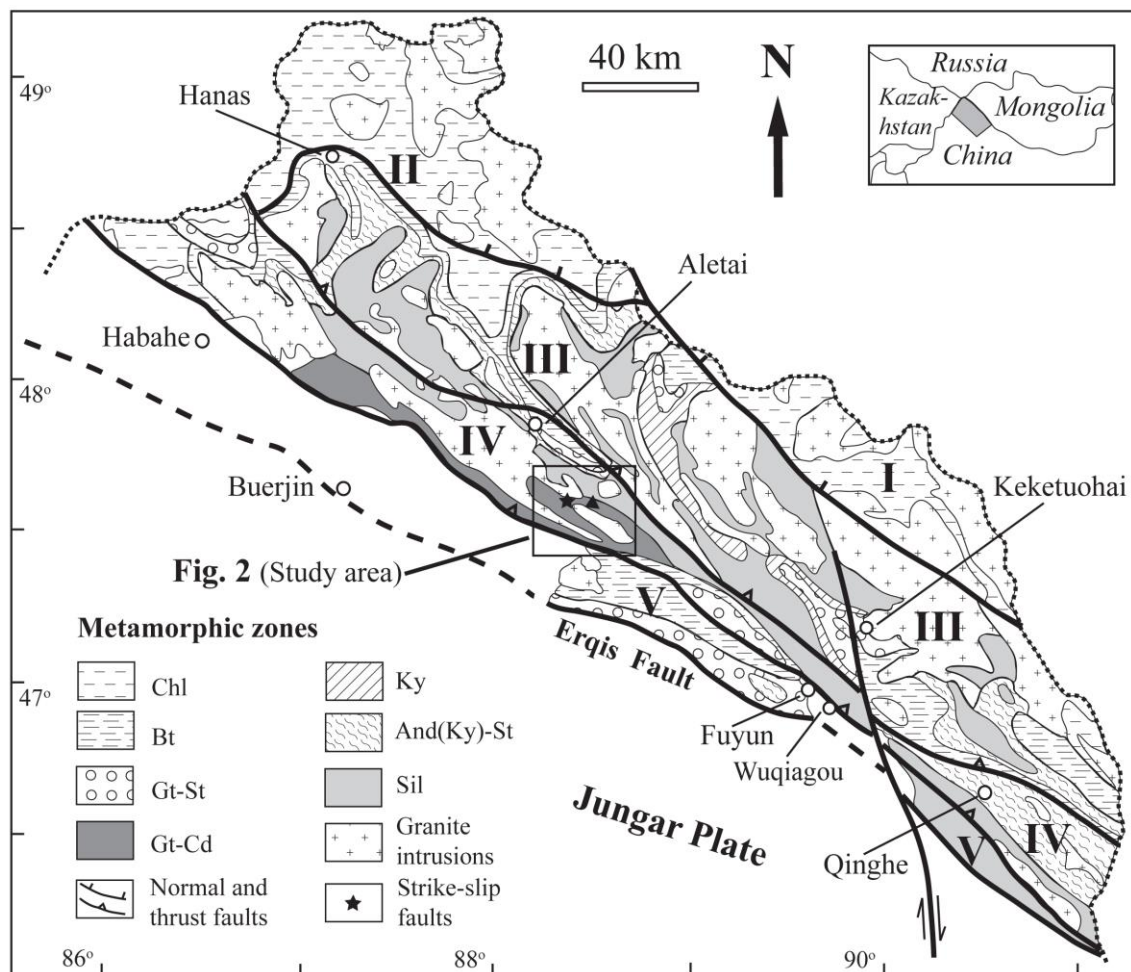634   **Table 3** SHRIMP U-Pb analysis results for zircons in the UHT metapelitic granulite.

635

636   **Table 4** Summary of the Permian isotopic ages reported from the Chinese Altai orogen.
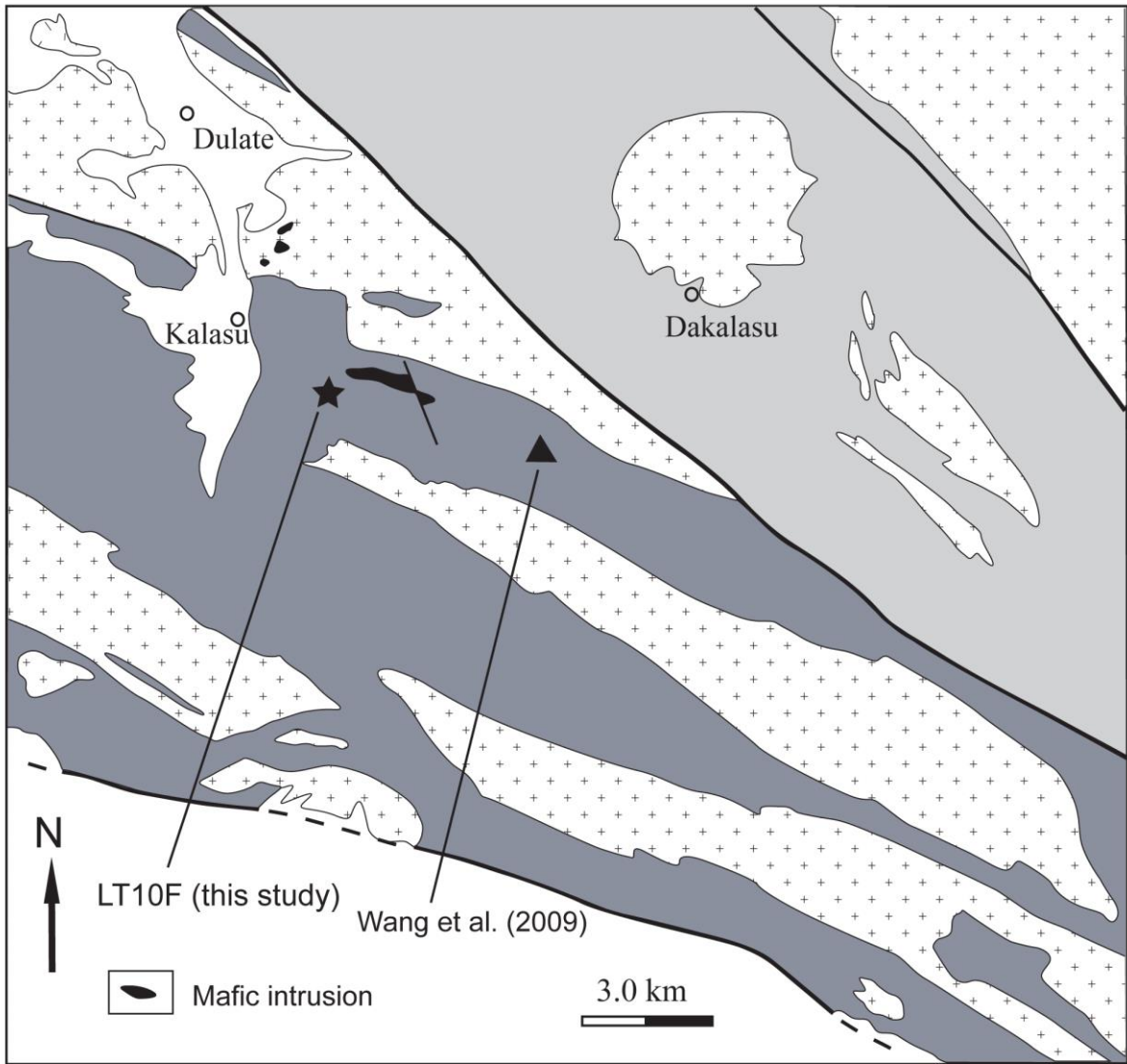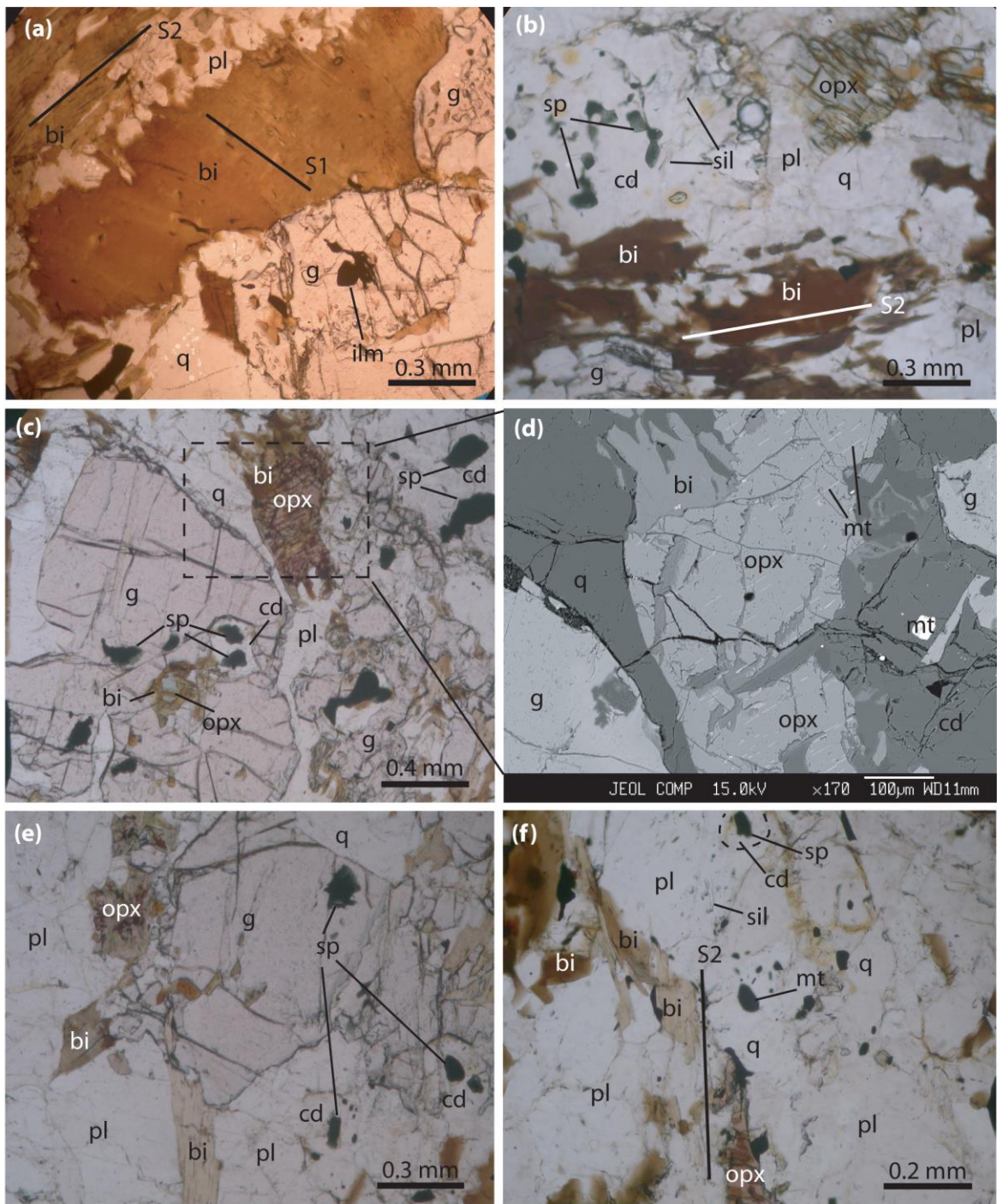
637

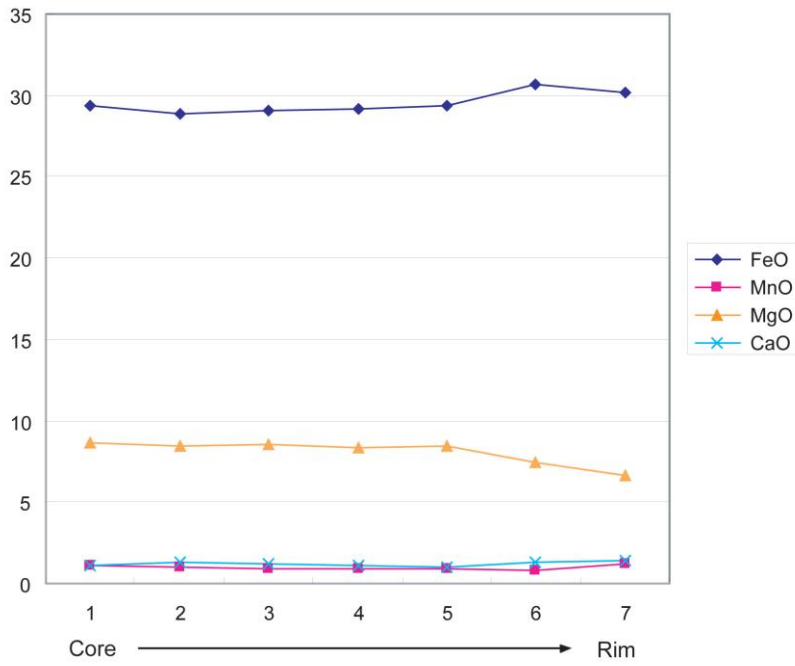638   **Fig. 1**

Fig. 2

648

Fig. 3.

649

650

651

652

653

654   Fig. 4

655

656   Fig. 5

29

NCKFMASHTO (+q+ilm)
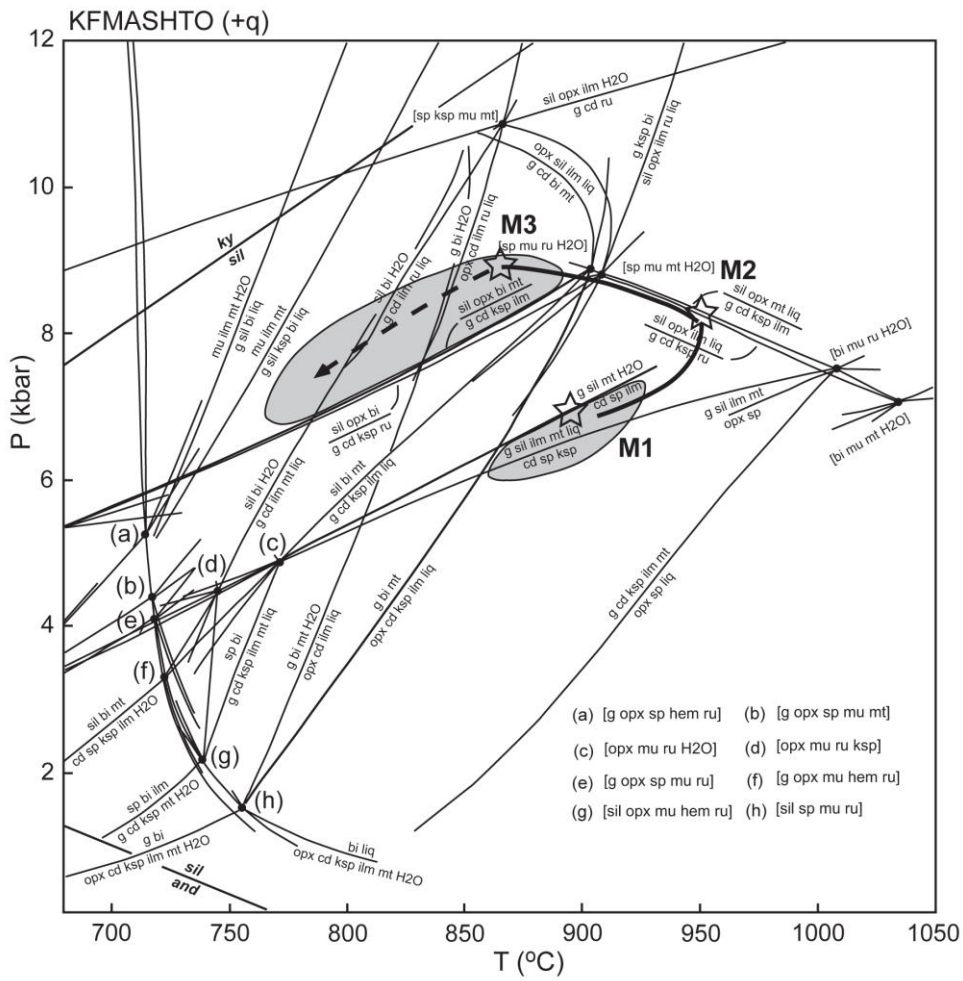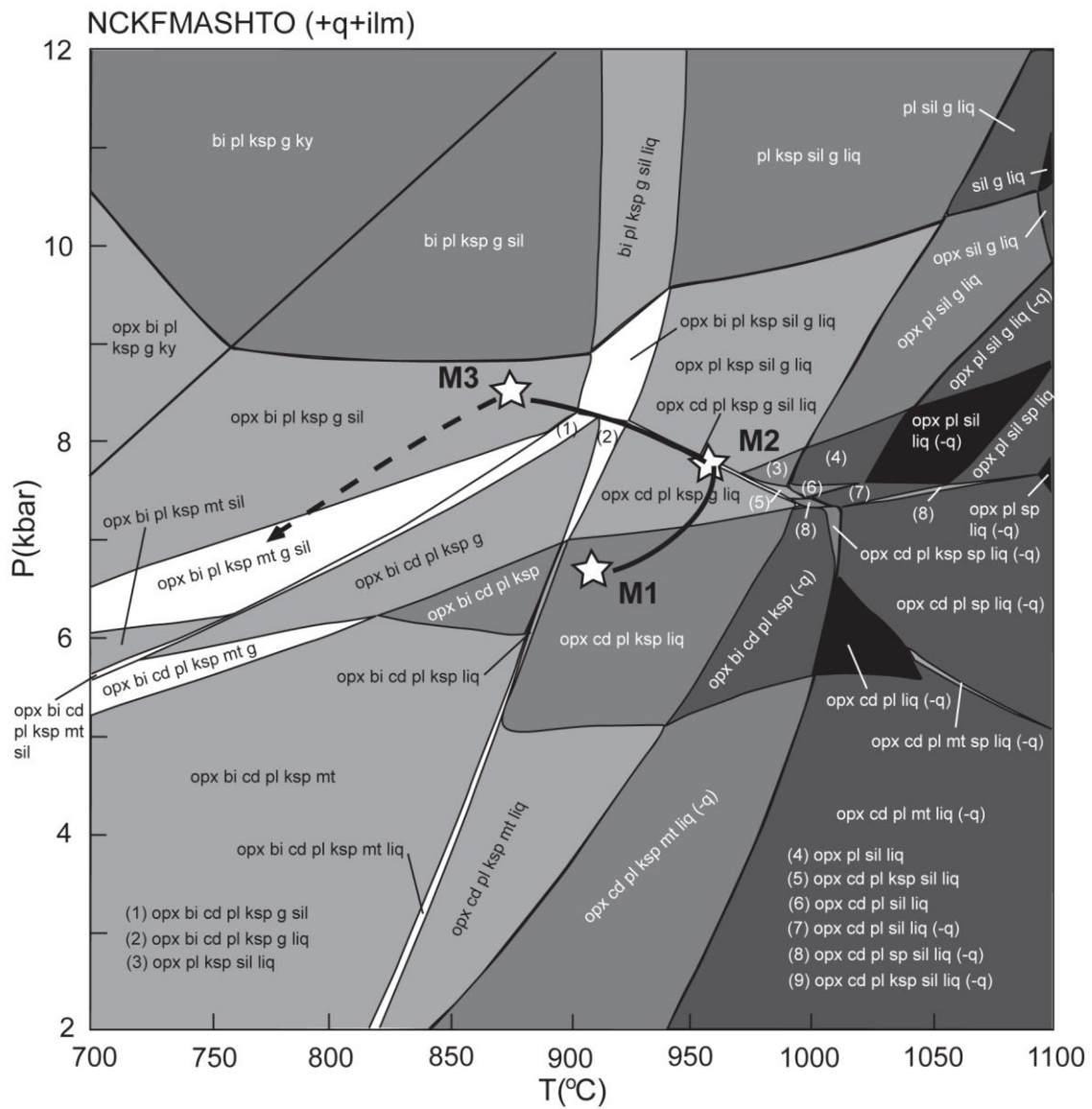
Fig. 6
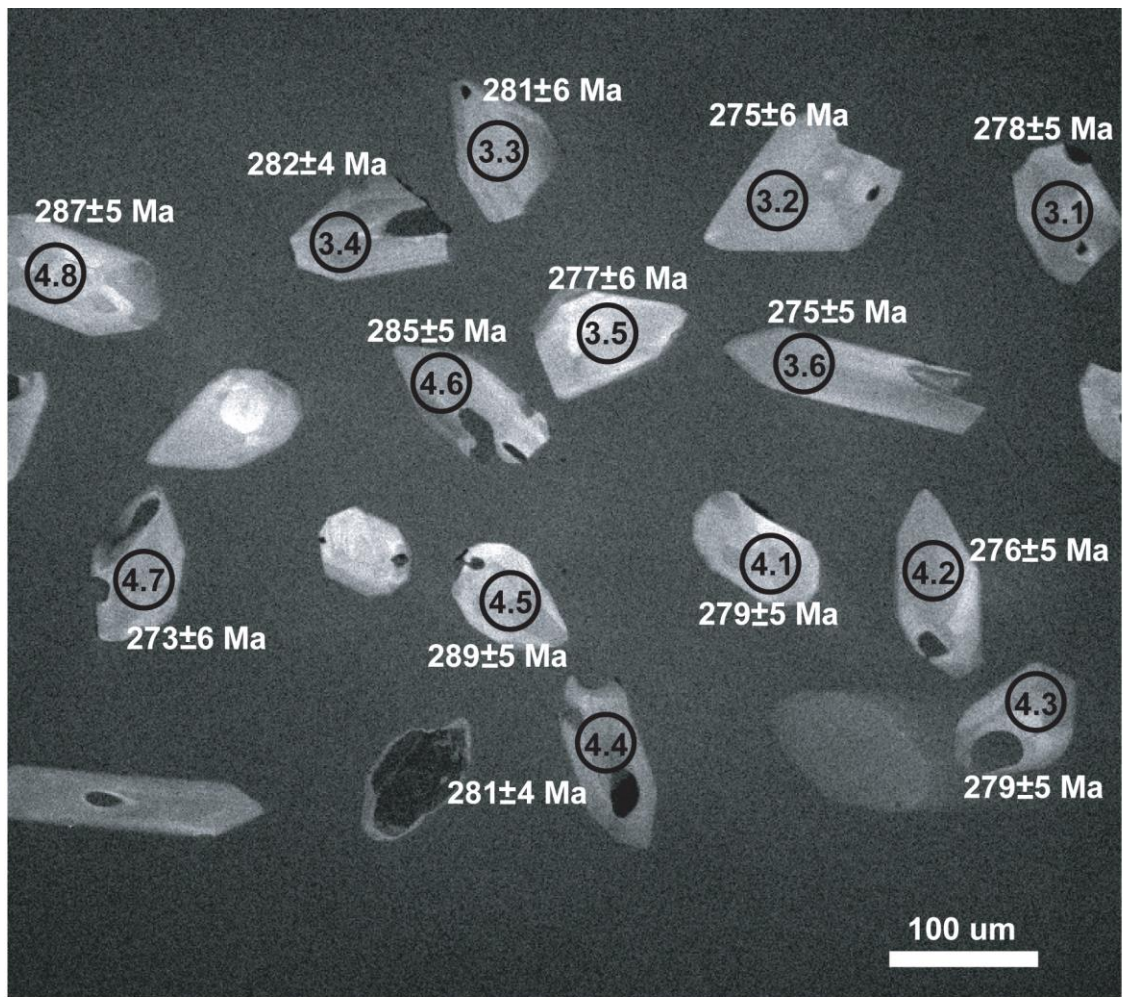
Fig. 7

666

667

668

669

670

671

672

673

Fig. 8

674

675

676

677

678

679
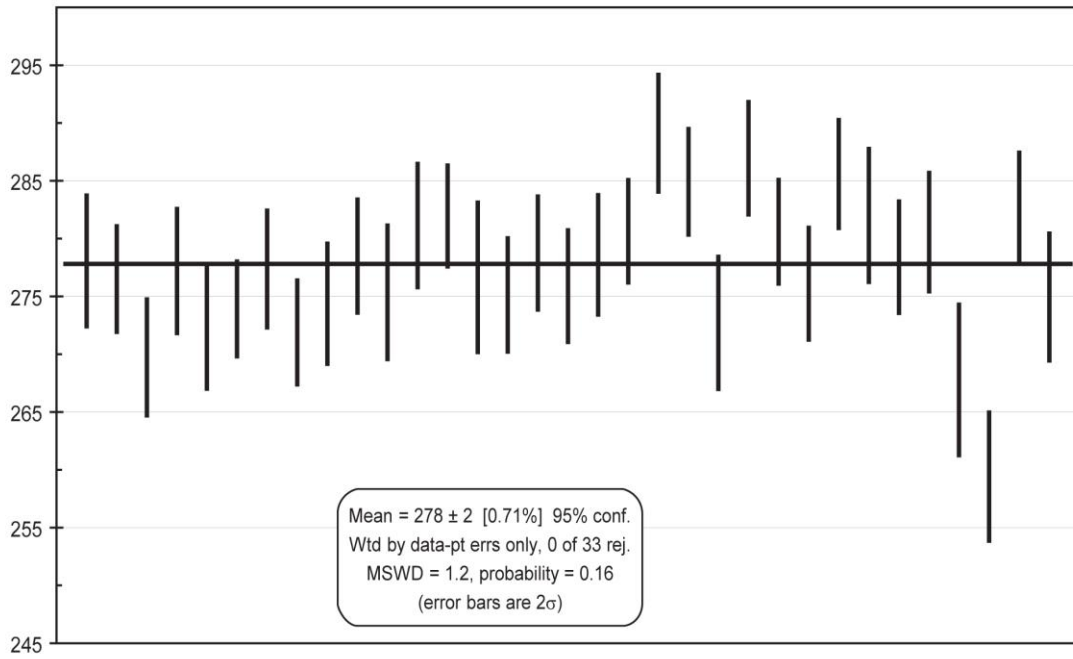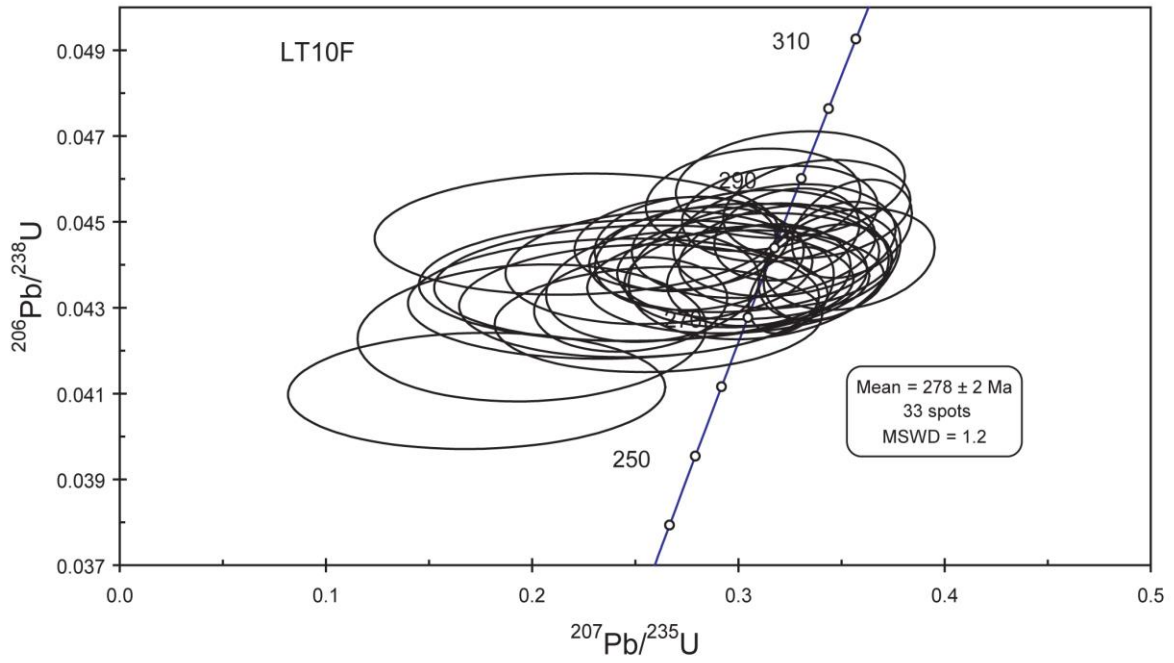
Table 1

	g(c)	g(m)	g(r)	opx(i)	opx(c)	opx(m)	opx(r)	opx(3)	sil	ilm(i)	sp(i)	sp(o)	mt(e)	cd(i)	cd	bi(i)	bi(c)	bi(r)	pl	pl
SiO_2	38.88	37.92	39.06	50.51	46.70	47.25	48.23	47.87	37.62	1.67	0.03	0.02	0.12	50.69	49.71	37.36	36.22	35.92	60.85	56.26
TiO_2	0.07	0.06	0.06	0.09	0.06	0.08	0.04	0.05	0.02	39.71	0.04	0.00	0.11	0.00	0.06	4.72	4.57	3.81	0.01	0.00
Al_2O_3	22.02	22.25	21.6	5.13	8.95	8.18	6.29	6.84	60.94	0.57	59.14	57.44	0.18	33.20	33.96	16.89	16.60	16.27	24.35	27.09
Cr_2O_3	0.03	0.01	0.03	0.00	0.00	0.00	0.00	0.01	0.04	0.05	0.25	1.16	2.16	0.00	0.00	0.09	0.12	0.09	0.00	0.02
Fe_2O_3	0.00	1.20	0.00	0.00	2.56	3.07	2.37	1.80	0.88	23.30	5.47	4.74	63.51	0.13	0.94	0.00	0.00	0.00	0.03	0.06
FeO	28.48	27.63	30.20	23.52	22.23	22.56	22.61	23.70	0.00	34.92	23.50	27.60	29.93	3.91	3.40	10.89	14.31	14.89	0.00	0.00
MnO	1.10	0.95	1.17	0.21	0.29	0.19	0.23	0.54	0.00	0.73	0.09	0.07	0.09	0.02	0.05	0.03	0.01	0.00	0.00	0.02
MgO	8.44	8.62	6.68	20.51	18.66	18.92	19.54	18.45	0.01	1.12	10.42	6.58	0.05	11.24	11.21	15.88	13.77	13.77	0.01	0.00
CaO	1.24	1.05	1.42	0.05	0.03	0.04	0.03	0.05	0.08	0.00	0.00	0.00	0.00	0.01	0.01	0.04	0.00	0.00	5.72	9.69
Na_2O	0.00	0.02	0.01	0.00	0.01	0.01	0.00	0.02	0.00	0.01	0.08	0.14	0.00	0.14	0.09	0.60	0.22	0.22	8.74	6.20
K_2O	0.00	0.00	0.00	0.00	0.01	0.00	0.00	0.00	0.00	0.00	0.00	0.01	0.00	0.01	0.00	9.81	10.14	10.84	0.16	0.09
ZnO											1.39	2.32								
Totals	100.26	99.59	100.23	100.02	99.25	100.00	99.11	99.15	99.59	99.75	99.86	99.60	96.15	99.34	99.43	96.32	95.96	95.82	99.85	99.41
O	12	12	12	6	6	6	6	6	10	3	4	4	4	18	18	11	11	11	8	8
Si	3.000	2.944	3.040	1.886	1.763	1.774	1.825	1.820	2.043	0.041	0.001	0.001	0.004	5.057	4.962	2.713	2.692	2.696	2.711	2.543
Ti	0.004	0.004	0.004	0.003	0.002	0.002	0.001	0.001	0.001	0.735	0.001	0.000	0.003	0.000	0.005	0.258	0.255	0.215	0.000	0.000
Al	2.003	2.037	1.982	0.226	0.398	0.362	0.281	0.307	3.901	0.017	1.890	1.895	0.008	3.905	3.997	1.446	1.455	1.440	1.279	1.444
Cr	0.002	0.001	0.002	0.000	0.000	0.000	0.000	0.000	0.001	0.001	0.005	0.026	0.064	0.000	0.000	0.005	0.007	0.005	0.000	0.001
Fe^{3+}	0.000	0.070	0.000	0.000	0.073	0.087	0.068	0.051	0.036	0.431	0.106	0.086	1.913	0.010	0.071	0.000	0.000	0.000	0.001	0.002
Fe^{2+}	1.838	1.795	1.966	0.734	0.702	0.708	0.716	0.754	0.000	0.719	0.542	0.660	1.002	0.326	0.284	0.661	0.890	0.935	0.000	0.000
Mn	0.072	0.062	0.077	0.007	0.009	0.006	0.007	0.017	0.000	0.015	0.002	0.002	0.003	0.002	0.004	0.002	0.001	0.000	0.000	0.001
Mg	0.971	0.998	0.775	1.141	1.050	1.058	1.102	1.045	0.001	0.041	0.421	0.275	0.003	1.671	1.668	1.719	1.525	1.540	0.001	0.000
Ca	0.103	0.087	0.118	0.002	0.001	0.002	0.001	0.002	0.005	0.000	0.000	0.000	0.000	0.001	0.001	0.003	0.000	0.000	0.273	0.469
Na	0.000	0.003	0.002	0.000	0.001	0.001	0.000	0.001	0.000	0.001	0.004	0.008	0.000	0.027	0.017	0.084	0.032	0.032	0.755	0.543
K	0.000	0.000	0.000	0.000	0.000	0.000	0.000	0.000	0.000	0.000	0.000	0.000	0.000	0.001	0.000	0.909	0.962	1.038	0.009	0.005
Zn											0.028	0.048								
Sum	7.993	8	7.965	3.999	4	4	4	4	5.988	2	3	3	3	11	11.01	7.801	7.819	7.902	5.030	5.008
X_{Mg}	0.346	0.357	0.283	0.609	0.599	0.599	0.606	0.581			0.437	0.294		0.837	0.855	0.722	0.631	0.622		
X_{Al}				0.113	0.199	0.181	0.141	0.154												

Table 2.

M1:	model 1	model 2	model 3	model 4	average
	T = 887 °C	T = 891 °C	T = 891 °C	T = 881 °C	T = 888 °C
	P = 7.0 kbar	P = 7.1 kbar	P = 7.1 kbar	P = 7.0 kbar	P = 7.1 kbar
M2:	model 1	model 2	model 3	model 4	average
	T = 984 °C	T = 962 °C	T = 966 °C	T = 959 °C	T = 968 °C
	P = 8.1 kbar	P = 7.9 kbar	P = 7.9 kbar	P = 7.9 kbar	P = 8.0 kbar

M3:	avP (kbar)	sd	avT (°C)	sd	cor	fit
	9.0	1.1	872	108	0.7	1.41

33

Table 3

Spot	% $^{206}Pb_c$	U	Th	Th/U	$^{207}Pb^*/^{206}Pb^*$	%	$^{207}Pb^*/^{235}U$	%	$^{206}Pb^*/^{238}U$	%	$^{207}Pb/^{206}Pb$ (Ma)	1s err	$^{208}Pb/^{232}Th$ (Ma)	1s err	$^{206}Pb/^{238}U$ (Ma)	1s err
LT10F-1.1	0.16	195	142	0.75	.0568	6.0	0.345	6.3	.0441	2.1	485.2	132	285.3	12	278.1	5.7
LT10F-1.2	0.29	152	114	0.78	.0566	6.0	0.342	6.2	.0438	1.7	476.0	132	287.5	12	276.5	4.6
LT10F-1.3	1.53	195	147	0.78	.0443	20.0	0.261	20.1	.0427	1.9	-91.7	490	255.0	26	269.7	5.0
LT10F-1.4	2.01	162	122	0.78	.0432	18.7	0.262	18.8	.0439	2.0	-158.0	464	249.7	24	277.2	5.4
LT10F-2.2	1.67	182	127	0.72	.0423	22.8	0.252	22.9	.0432	2.0	-206.8	572	263.2	30	272.4	5.4
LT10F-2.3	0.15	279	237	0.88	.0544	3.9	0.326	4.2	.0434	1.5	388.1	87	279.3	8	273.9	4.1
LT10F-1.5	1.56	156	125	0.83	.0508	14.2	0.308	14.3	.0440	1.9	231.9	327	273.3	21	277.4	5.1
LT10F-1.6	1.83	247	196	0.82	.0417	12.4	0.248	12.5	.0431	1.7	-243.4	312	239.3	15	271.9	4.5
LT10F-1.7	2.34	212	162	0.79	.0431	13.1	0.258	13.2	.0435	1.9	-161.4	325	238.1	18	274.4	5.2
LT10F-3.1	1.85	165	143	0.90	.0462	11.7	0.281	11.9	.0441	1.8	7.3	283	257.8	15	278.5	4.9
LT10F-3.2	2.45	168	118	0.73	.0423	28.3	0.254	28.3	.0436	2.1	-210.2	710	250.9	37	275.3	5.8
LT10F-3.3	0.53	202	147	0.75	.0524	10.9	0.322	11.0	.0446	1.9	305.0	248	288.9	19	281.1	5.3
LT10F-3.4	0.43	221	176	0.82	.0525	7.0	0.324	7.2	.0447	1.6	306.6	159	277.0	12	282.0	4.4
LT10F-3.5	1.76	127	88	0.72	.0512	13.2	0.310	13.4	.0438	2.4	251.9	304	269.8	20	276.6	6.5
LT10F-3.6	2.69	195	137	0.73	.0497	15.8	0.299	15.9	.0436	1.8	180.4	368	269.2	25	275.1	4.9
LT10F-4.1	1.69	144	109	0.78	.0532	10.6	0.324	10.8	.0442	1.8	337.7	241	272.0	18	278.7	4.9
LT10F-4.2	1.78	164	118	0.74	.0503	12.7	0.304	12.8	.0437	1.8	211.2	294	248.3	20	275.9	4.8
LT10F-4.3	2.49	133	102	0.79	.0489	15.5	0.298	15.6	.0442	1.9	145.0	363	260.1	23	278.6	5.2
LT10F-4.4	1.63	246	178	0.75	.0444	12.4	0.272	12.5	.0445	1.6	-89.7	305	255.8	16	280.6	4.4
LT10F-4.5	1.40	132	101	0.79	.0514	11.1	0.325	11.3	.0459	1.8	259.9	256	280.0	18	289.1	5.0
LT10F-4.6	0.96	213	154	0.75	.0514	9.6	0.320	9.8	.0452	1.6	258.0	222	283.3	16	284.9	4.6
LT10F-4.7	2.59	145	107	0.77	.0405	27.7	0.242	27.8	.0432	2.1	-316.2	711	254.7	33	272.7	5.7
LT10F-4.8	1.58	143	116	0.84	.0489	11.0	0.307	11.2	.0455	1.7	145.2	259	288.4	14	286.9	4.9
LT10F-4.9	1.48	209	155	0.77	.0447	10.4	0.274	10.6	.0445	1.6	-71.9	255	259.7	15	280.6	4.5
LT10F-5.1	0.94	146	122	0.86	.0514	9.3	0.310	9.5	.0438	1.8	257.3	214	270.2	13	276.1	4.8
LT10F-5.2	1.66	209	173	0.85	.0541	8.7	0.338	8.9	.0453	1.7	376.3	196	267.9	13	285.6	4.7
LT10F-5.3	3.50	118	81	0.71	.0359	29.1	0.221	29.2	.0447	2.1	-636.7	797	236.7	33	282.0	5.7
LT10F-5.4	1.00	111	77	0.72	.0582	7.5	0.354	7.7	.0441	1.8	536.8	163	305.1	13	278.4	4.8
LT10F-5.5	1.67	113	78	0.72	.0501	12.5	0.307	12.7	.0445	1.9	200.4	291	276.4	22	280.6	5.1
LT10F-5.6	3.65	134	97	0.75	.0342	27.8	0.200	27.9	.0424	2.5	-775.5	784	217.6	29	267.8	6.5
LT10F-6.1	4.85	95	68	0.74	.0306	34.8	0.173	34.9	.0411	2.2	-1101.3	1056	206.8	32	259.4	5.5
LT10F-6.2	0.85	131	90	0.71	.0574	5.1	0.355	5.4	.0448	1.7	508.2	113	281.4	11	282.8	4.7
LT10F-6.3	2.02	176	124	0.73	.0423	26.3	0.254	26.4	.0436	2.0	-208.2	661	240.6	33	274.9	5.5

689
690

Table 4

Locations	Rocks	Methods	Ages (Ma)	References
Qinghe	Gneiss	SHRIMP	281 ± 3	Hu et al. (2006)
Fuyun	Mafic granulite	SHRIMP	279 ± 6	Chen et al. (2006b)
Fuyun	Gneiss	in situ Th-Pb	278 ± 9, 275 ± 8	Briggs et al. (2007)
Altai-Qinghe	Gneiss	CHIME	261-268	Zheng et al. (2007)
Kalasu	Pelitic granulite	SHRIMP	293 ± 2	Wang et al. (2009)
Fuyun	Pelitic granulite	LA-ICP-MS	269-292	Li et al. (2012)
Qinghe	Gabrro	SHRIMP	272 ± 2	Zhang et al. (2010)
Fuyun-Qinghe	Granite	SHRIMP	283 ± 4	Zhang et al. (2012)
Kalatongke	Mafic Complex	SHRIMP	287 ± 5	Han et al. (2004)
Huangshandong	Mafic Intrusion	SHRIMP	269 ± 2	Zhou et al. (2004)
E Junger	Granitoid	Rb-Sr	294 ± 4	Chen & Jahn (2004)
Lamazhao	Granite	SHRIMP	276 ± 9	Wang et al. (2005)
Fuyun	Granite	TIMS	281 ± 5, 275 ± 2	Tong et al. (2006a)
Qinghe	Granite	SHRIMP	283 ± 4	Zhou et al. (2007)
Fuyun	Mafic intrusion	SHRIMP	257, 280	Chen & Han. (2006)

691

692